



Optimization of electron scattering from random potential barriers on the surface of topological insulators

Scientific research paper

Hamid Dehnavi¹, Mehdi Saadat^{1,2*}

¹*Department of Physics, North Tehran Branch, Islamic Azad University, Tehran, Iran*

²*Department of Physics, Shahid Rajaei Teacher Training University, Tehran, Iran*

ARTICLE INFO

Article history:

Received 14 December 2021

Revised 9 January 2022

Accepted 13 January 2022

Available online 27 January 2022

Keywords:

Topological insulators
Random potentials,
Transmission coefficient
Conduction
Potential barriers

ABSTRACT

Optimization of electron scattering has been investigated using random potential barriers. Random potential barriers can be defined in two situations. In the first case when line defects are placed regularly on the surface of the topological insulator, but their strength changes randomly. In the second case when the potential barriers strength are constant while location of line defects on the surface of the topological insulator are changing randomly. To obtain better results, probability of transmission in the random potential states are calculated N times. These N values are averaged and the result is compared with the probability of transmission in the regular case. It seems that, in propagating of incident electrons for some amounts of incident energy, number of defects, strength of potential, even direction of propagation, the results are close to the values obtained for the regular case. For some amounts of incident energy or some structural parameters significant differences are seen. We encounter large variation in electrical conduction, when the location of potential barriers change randomly, relative to the case that strength of random potential is changed. In fact, the reason for higher electrical conductivity is the constructive interference that occurs between propagating electron waves. Therefore, in the presence of such random potential barriers, the conduction and transmission of incident electrons have been improved.

1 Introduction

Recently, a new quantum behavior in the field of condensed matter physics and materials science has attracted much attention. The materials in which this strange behavior is observed are known as topological insulators [1], [2]. These materials with surface states with and without energy gap in the bulk of insulation result from a strong spin-orbit interaction and time-reversal symmetry [3], [4], [5], [6]. In other words, the superficial states of conduction are maintained in such

materials as long as the time-reversal symmetry is not broken [7], [8], [9].

Impurities on the surface of topological insulators cause scattering of the wave function showing interesting electronic properties [10], [11], [12], [13]. Impurities in fact, in the presence of an electric field and a spin-orbit coupling, cause electron scattering. This effect has been observed experimentally in thin layers of GaAs and InGaAs [14]. Impurities also deform the 3D Dirac cone in Bi_2Se_3 [13]. In other words, magnetic impurities can create a local energy

*Corresponding author.

Email address: Saadat@sru.ac.ir

DOI: 10.22051/jitl.2022.38844.1064

gap by suppressing the local state density and inducing an interaction RKKY (Ruderman, Kittel, Kasuya, Yosida) in the system [10], [11].

Surface defects and ripples in topological insulators can also scatter Dirac electrons. Bismuth-based topological insulators such as Bi_2Te_3 and Bi_2Se_3 [15] are inexpensive materials that have excellent electrical conductivity on their surfaces [16], [17]. Okada et al. [18] created a series of local ripples on the surface of Bi_2Te_3 . They proposed 2D defects to control the properties of Dirac fermions in topological insulators. Such local ripples can be created by periodic buckling during sample growth or by chain induction through a piezoelectric crystal [18].

One-dimensional periodic potentials on the surface of these materials are responsible for trapping surface electrons and displacing energy levels. In this case, regular linear defects (local ripples) are modeled by the delta-function potential [19], [21]. Using an approach of quantum mechanics, Ting and An investigated the scattering of surface states of a single potential barrier in Bi_2Te_3 by the hexagonal warping effects [20]. They showed that, passing of the incident electrons under certain conditions when line defect is along ΓM can be perfect, and since there is a limited possibility for the reflection of electrons, when the incident wave has a component along ΓK its Fermi energy increases. The warping parameter plays an important role in changing the constant energy contour (CEC) from a circle to a hexagon and then to a snowflake shape with sharp corners. The torsion of the CEC is modulated by an external magnetic field [22], [23]. However, at high energies, where the warping effect is strong, it may significantly increase the electrical conductivity and thus the induction passage channels shown by the CEC snowflake shape [23]. The influence of the local delta-function potentials in two and three dimensions along the ΓK on the transmission of incident electrons in Bi_2Te_3 has been reported [19]. We have also reported up to 20 barriers in both directions ΓK and ΓM in our previous work [24]. The results show that the electrical conductivity fluctuations with strong delta-function potential and that the electronic transmission on the surface of topological insulator can be controlled by structural parameters.

In this paper, we try to investigate electronic transmission on the surface of a topological insulator in presence of random ripples. We consider a series of line defects with values of random strength and random distance from each other in two directions ΓK and ΓM . The transmission coefficients as well as the conductivity of the incident electrons are calculated for different structural parameters such as: number of potential barriers, strength of potential, distance of barriers, and the energy of the incident electron in two modes. At first the strength of potential barriers and then location of potential barriers varies randomly. In each case we obtain the values of transmission coefficients and conduction N times, then we calculate the mean values, and finally the results are compared to the cases in which the ripples were regular.

2 Method

We consider 3D topological insulator Bi_2Te_3 with strong warping effect and Dirac cone on the surface. By adjusting the Fermi level of the surface states, we can avoid the interaction between the surface and volume states [25]. Single particle Hamiltonian for surface electrons with torsional hexagonal states can be expressed as follows:

$$H(p_x, p_y) = v(p_x \sigma_y - p_y \sigma_x) + \lambda(p_x^3 - 3p_x p_y^2) \sigma_z, \quad (1)$$

since $p_x = -i\hbar \partial_x$ and $p_y = -i\hbar \partial_y$ are the 2D momentum operators of surface electrons, and σ_j ($j = x, y, z$) are the Pauli matrices. $v = 2.55 \text{ eV} \cdot \text{\AA}$ is the Fermi velocity and $\lambda = 250 \text{ eV} \cdot \text{\AA}^3$ is the warping parameters [25], [26]. For a more physical expression of the electron wave function propagated in the $\Gamma K(x)$ direction, we express it as follows:

$$\tilde{\psi}_k(\vec{r}) = \frac{1}{\sqrt{|v_x(\vec{k})|}} \psi_k(\vec{r}) \quad (2)$$

where $\psi_k(\vec{r})$ is the eigenstate of the Hamiltonian expressed by Eq. (1) and $v_x(\vec{k})$ is the electron group velocity along the x-axis [20], [24].

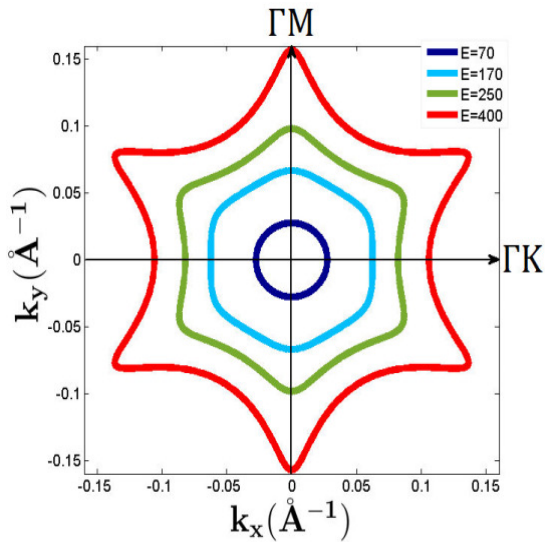


Figure 1. Fixed energy contours are displayed in the plane $k_x - k_y$ for energies (70, 170, 250, and 400) meV.

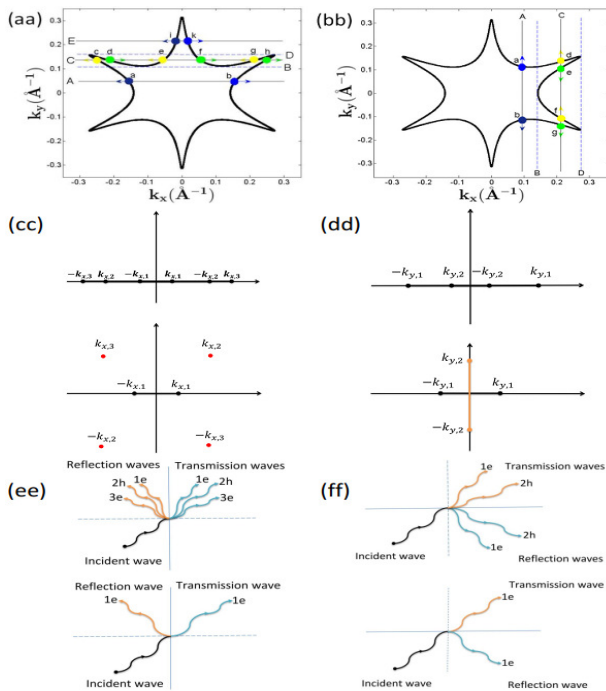


Figure 2. The roots are investigated in two states on a constant energy contour when the contour is hexagonal. The diagrams (aa), (cc), and (ee) show six roots. In the diagrams (bb), (dd), and (ff) four roots are shown [20].

Figure 2, the CEC snowflake states show the points more clearly on it; the amount of Fermi energy has been taken very large. In diagram (2aa), as we can see, the direction of wave motion is considered in the

direction of the momentum k_x , lines A and E intersect the energy contour at only two points (a,b) or (i,k), which shows that for values of k_y according to diagram (2aa) we will have only two real roots and four mixed roots. For certain values of k_y that this range is marked on CEC using dashes B and D, the line C intersects the contour at six points (c,d, e,f,g,h) which shows that the energy equation in k_x direction has six real roots for specific values of k_y . Graph (2cc) shows the state of six real roots and two real roots in the $k_x - k_y$ plane. In diagram (2ee), schematically, the case where we have two real roots in which the incident wave according to diagram (2aa) has a certain k_y momentum, scattered by a defect, we have a reflected wave and a transmission wave. In the case that we have six real roots, the incident electron wave has a certain amount of momentum k_y as shown in diagram (2aa), scattered by a defect, we have three reflected waves and three passing waves. In diagram (2bb), in which the direction of motion of the incident electron wave is in the k_y direction, for values of k_x (zero momentum value is indicated by the dashed line B) line A intersects the CEC at only two points, which shows that the energy equation in terms of k_y has only two real roots and two purely imaginary roots. The range of momentum is shown in diagram (2bb) by the dashed lines B and D, line C intersects the CEC at four points (d,e,f,g), which shows that the energy equation has four real roots. Diagram (2dd) shows the state of four real roots and two real real roots on the $k_x - k_y$ plane. Diagram (2ff) schematically shows the incident electron wave has had a specific motion according to diagram (2bb), when an electron encountered a defect on the surface of insulator in the k_x direction, it will have only one reflected wave and one transmission wave. If the incident wave according to diagram (2bb) has had a momentum k_x in the range between the dashed lines B and D, we will have two reflected waves and two transmitted waves. According to the shapes (2cc) and (2dd) the roots have positive and negative pairs. When all the roots are real, according to the diagrams (2ee) and (2ff) a wave travels in directions k_x and k_y in the a holelike form [24].

3 A SUPERLATTICE ALONG $\Gamma K(x)$ or $\Gamma M(y)$

Here ripply structures include N delta-function potential with random potential strength and random distance from each other on the surface of topological insulator Bi_2Te_3 , along X or Y axis. The wave function of electron in the region $(n-1)d < x < nd$, is the eigenstate of equation $\{H(-i\partial_x, k_y) + \sum_{n=0}^{N-1} U\delta(x-nd)\}\psi_k^{(n)}(\vec{r}) = E\psi_k^{(n)}(\vec{r})$. Because of this, the eigenvalue equation is a third-order partial differential equation relative to x , so we will have three boundary conditions [20], [24]. After applying the boundary conditions on the wave function and using the 6×6 transfer matrix, the relationship between the n^{th} coefficient and the $(n+1)^{th}$ coefficient is obtained [24].

Note that the Hamiltonian is not symmetric under transformation $p_x \leftrightarrow p_y$, therefore, the electron wave function in the region $(n-1)d < y < nd$, is an eigenstate of a second-order partial differential equation relative to y : $\{H(k_x, -i\partial_y) + \sum_{n=0}^{N-1} U\delta(y-nd)\}\psi_k^{(n)}(\vec{r}) = E\psi_k^{(n)}(\vec{r})$, so two boundary conditions will be obtained [20], [24]. By applying boundary conditions to the wave function, a 4×4 transfer matrix is obtained, which relates the n^{th} coefficient to the $(n+1)^{th}$ coefficient [24]. According to Fig. 2, if all roots are real, the transmission coefficient T is the sum of $|t|^2$'s. If two roots are real, the transmission coefficient T is only $|t_1|^2$ [20]. In the case of N barriers, when the potential strength is random, every one receives a random value in the range $(U \pm 0.1)eV \cdot \text{\AA}$, then the transmission coefficient is calculated. This operation is repeated N times and N values are obtained for the transmission coefficients before averaging the values. Also when the distances between potential barriers are random, in each calculation, location of barriers receives arandom values in the range $(d \pm 0.1)\text{\AA}$. This operation can be repeated few times to obtain few transmission coefficients. Averaging these values we draw the transmission coefficient diagram in terms of $d(\text{\AA})$ or $U(eV \cdot \text{\AA})$. We observe fluctuations in the transmission diagram and that we can compare it with the transmission diagram of a regular superlattice. The following equation is used to calculate $\bar{T}(E, \theta)$:

$$\bar{T}(E, \theta) = \frac{1}{N} \sum_i^N T(E, \theta) \quad (3)$$

To calculate the electrical conductivity of topological insulators in the $\Gamma K(x)$ direction, potential strength of each N barriers or the distance of the barriers are random values in the range $(U \pm 0.1)eV \cdot \text{\AA}$ and $(d \pm 0.1)\text{\AA}$. This operation can be repeated few times before averaging the obtained values for electrical conductivity. The following equations are used to calculate the electrical conductivity and its average [19]:

$$G/G_0 = \int_0^{\pi/2} T(E, \theta) \cos\theta d\theta \quad (4)$$

$$\overline{G/G_0} = \frac{1}{N} \sum_i^N G/G_0 \quad (5)$$

where $\theta = \arctan(k_y/k_x)$ indicates the angle of incident electron and G_0 is a constant.

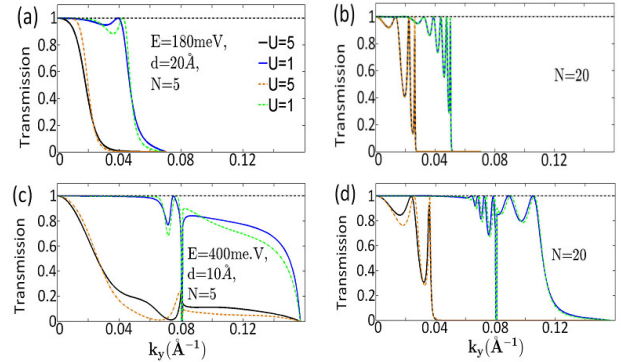


Figure 3: Transmission coefficients in terms of momentum k_y . Ripples are parallel to x axes while N is the number of them distributed randomly in direction y .

4 Results and discussion

In Fig. 3 the lattice constant d in diagrams (a) and (b) is a random value in range $(20 \pm 0.1)\text{\AA}$ in solid line curves, and a constant value, 20\AA for dashed line curves. The lattice constant d in diagrams (c) and (d) is a random value in the range $(10 \pm 0.1)\text{\AA}$ for solid curves and a constant value, 10\AA for dashed line curves. In diagrams (a) and (b) the incident electron energy is 180meV and 400meV in diagrams (c) and (d). The number of line defects in diagrams (a) and (c) is $N=5$ and $N=20$ in diagrams (b) and (d). Dependence of energy and wave number of the incident electron in transmission through the line defects with random

lattice constant in Bi_2Te_3 , plotted in Fig. 3. The transmission coefficient in terms of k_y at two incident energies $E = 180\text{meV}$ and $E = 400\text{meV}$ for 5 and 20 barriers expanded along the y -direction are shown. Location of potential barriers takes a random value in the range $(20 \pm 0.1)\text{\AA}$ in diagrams (3a) and (3b) and takes a random value in range $(10 \pm 0.1)\text{\AA}$ in diagrams (3c) and (3d). Each point of the solid black lines with $(U = 5\text{eV.\AA})$, and blue $(U = 1\text{eV.\AA})$ are obtained 50 times, averaging these values leads to \bar{T} which is shown in the diagrams. The values of T in the dashed line diagrams of Fig. 3, with the same potential strength $(1.5)\text{eV.\AA}$, are plotted in diagrams (3a), (3b) for lattice constant $d = 20\text{\AA}$ and in diagrams (3c), (3d) for lattice constant 10\AA . In this figure for a smaller number of barriers there is more difference between \bar{T} and T , because with increasing the number of barriers, the random values increase and as a result, the mean value is averaged with more numbers, which bring it closer to a fixed value. By increasing the incident energy for less number of barriers, the average values show a better transmission coefficient than the fixed transmission values. The reason is due to the constructive interference modes [28], caused by the random spacing of the barriers. At the peaks of the transmission coefficient curves, the conditions for the transmission of electrons in the steady state are better seen.

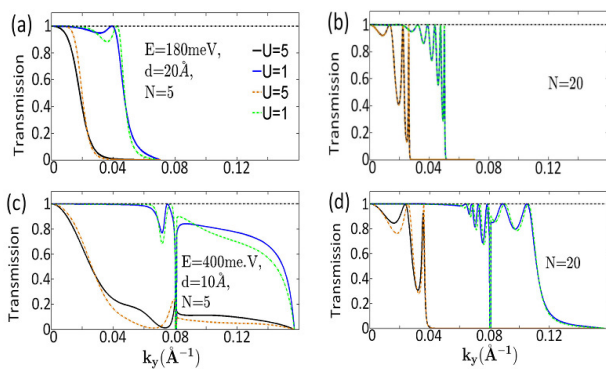


Figure 4: Transmission coefficients in terms of momentum k_x . Ripples are parallel to the y axes while N is the number of them, distributed randomly in direction x . Because in the random mode, destructive interference takes place between the transmitted and reflected waves.

In Fig. 4 the distance of potential barriers in solid curves is in the range $(10 \pm 0.1)\text{\AA}$. For dashed line

curves the constant value is 10\AA . The number of barriers in diagrams (a) and (c) are $N = 5$ and in diagrams (b) and (d) are $N = 20$. The potential strength of solid line and dashed line curves is $(1,5)\text{eV.\AA}$. Incident energy of electron in diagrams (a) and (b) is $E = 170\text{meV}$ and in diagrams (c) and (d) is 250meV . In Fig. 4 line defects were extended along the x -direction. As it is shown in the diagrams, transmission coefficients in the random lattice constant case and regular lattice constant case are plotted in terms of k_x at two incident energy, one less than the critical limit $E = 170\text{meV} (< 180\text{meV})$ and the other more than the critical limit $E = 250\text{meV}$. Like Fig. 3, the lattice constant d selects random values in the range $(10 \pm 0.1)\text{\AA}$. Note that the incident electron moves in the direction y , so for low and high energies and two barriers, there is a little difference between T and \bar{T} in graph (d) for $U = 1\text{eV.\AA}$ except at the peaks. This slight difference may be due to the fact that the sharp peaks became smooth in the averaging process. In diagram (4a) since the peaks are not sharp, there is no noticeable difference between the averaged transmission coefficient in the random case and the transmission coefficient in the regular case. While in diagrams (4b) and (4d) where $U = 5\text{eV.\AA}$ there are more sharp peaks that have been averaged that lead to correct transmission coefficients. In diagram (4d), where the potential strength is $U = 1\text{eV.\AA}$ after averaging, a significant decrease can be seen in the transmission coefficient relative to the regular case which is due to non-constructive interference modes. For more number of barriers, diagrams (4b) and (4d), with increasing number of peaks, we see a decrease in the average amount of transmission coefficient at the same peak.

By comparing Figs. 3 and 4, we see that, amount of transmission coefficient through random defects is strongly dependent on the direction in which they are located. In Fig. 4, random values of the lattice constants (distance between potential barriers) that lead to the average value of \bar{T} have less influence than T due to regular superlattice except for diagram (4d) with $U = 1\text{eV.\AA}$ which is an exception. In Fig. 3 this effect is more visible, which is due to the properties of electrons transmitting through the line defects in the x and y directions. Source of these differences are in

their boundary conditions and also Hamiltonian asymmetry under the transformation $k_x \leftrightarrow k_y$ [24].

Figure 5, the potential strength of solid line curves are in the range $(5 \pm 0.1)eV.\text{\AA}$ while for dashed line curves, the of potential height of barriers is $5eV.\text{\AA}$. The distance between potential barriers for solid line and dashed line curves is $(10,20)\text{\AA}$. The energy of the incident electron in diagrams (a) and (b) is $180meV$ and in diagrams (c) and (d) is $400meV$. Number of potential barriers, which is in the y -direction, in diagrams (a) and (c) are $N=5$ and in diagrams (b) and (d) are $N=20$.

Figure 6 potential barriers are in the x -direction, there are two categories of solid line and dashed line graphs. The heights of random potential barriers are in range $(5 \pm 0.1)eV.\text{\AA}$ while the height of regular potential barriers is $5eV.\text{\AA}$. The distance between potential barriers for both categories of curves is $(10,15)\text{\AA}$. In diagrams (a) and (b) energy of the incident electron is $170meV$ and in diagrams (c) and (d) is $250meV$. The number of defect lines in diagrams (a) and (c) are $N=5$ and in diagrams (b) and (d) are $N=20$.

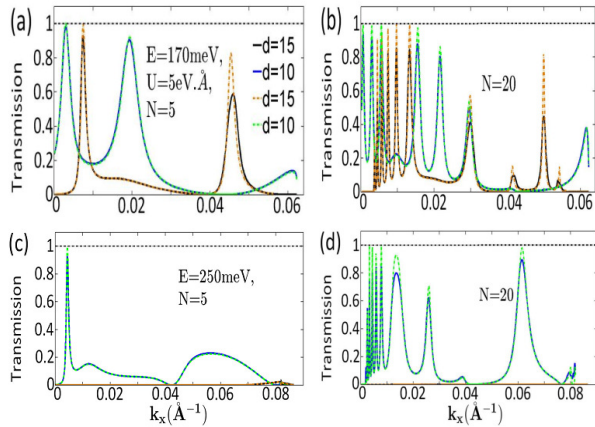


Figure 5: The transmission coefficient for barriers of random height. Ripples are parallel to x axes and N is the number of them in direction y .

In Figs. 5 and 6 instead of random distance between barriers, we have selected the strength of potential barriers randomly. In Fig. 5 we consider the random potential barriers in the y -direction. Transmission coefficient in terms of k_y are plotted for two set of curves in each graph. Solid curves which are the mean transmission coefficient have been calculated using random values for potential strength in range $U = (5 \pm$

$0.1)eV.\text{\AA}$ and dashed line curves are transmission coefficient using a fixed value $U = 5eV.\text{\AA}$ for barriers height. In both cases distance between barriers are $(10,20)\text{\AA}$. At incident energies lower than critical limits, by reducing the distance between potential barriers from 20\AA to 10\AA , the difference of mean value of transmission coefficients \bar{T} , and T increase. But at higher incident energies the difference between \bar{T} and T decreases. Specially in the case that the number of barriers increases, the difference in the transmission peaks is obvious, which can be due to the constructive interference of transmitted and reflected electron waves. Dependence of incident energy and spatial distance between the superlattice line defects in Bi_2Te_3 are plotted in Fig. 6 for random and fixed potential strengths.

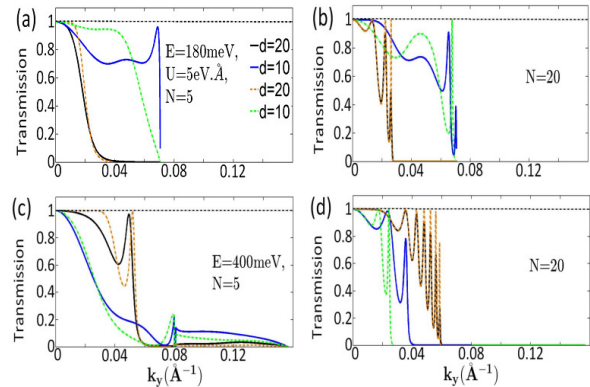


Figure 6. The transmission coefficient for barriers of random height. Ripples are parallel to the y axes while N is the number of them in direction x .

Transmission coefficients in terms of k_x for two incident energies $E = 170meV (< E_c)$ and $E = 250meV (> E_c)$ are shown for $N = 5$ and $N = 20$ line defects extended along the x -direction. The amount of potential strength that each barrier selects randomly is in the range of $(5 \pm 0.1)eV.\text{\AA}$. Solid curves show the mean value of the transmission coefficient, \bar{T} , and dashed line curves show the value of the transmission coefficient of regular superlattice, T , for two fixed lattice constant $(10,15)\text{\AA}$. When electron waves propagate in the x -direction, the difference between \bar{T} and T is in sharp peaks. For low number of barriers of (graphs (6a) and (6c)) the difference between \bar{T} and T decreases with increasing incident electron energy. Also for more number of defect lines (graph (6b) and

(6d)) transmission coefficients decrease with increasing of the incident electron energy which leads to sharp peaks. This small difference, is due to low effect of random potential strength on the interference modes. Solid line curves are mean values of electrical conductivity for random barriers in terms of distance between barriers and potential strength while dashed line curves are electrical conductivity for regular superlattice. Diagram (a) is the mean value of the electrical conductivity for random potential strength in the range $(5 \pm 0.1)eV \cdot \text{\AA}$, and the dashed line curve is electrical conductivity for fixed value $U = 5eV \cdot \text{\AA}$. Diagram (b) is the mean value of the electrical conductivity for random distance between barriers in range $(10 \pm 0.1)\text{\AA}$ and dashed line curve is electrical conductivity for fixed value $d = 10\text{\AA}$. The incident energies for both categories in black and blue curves are 180meV and 400meV respectively.

On the surface of topological insulators, electrical conductivity can be checked by the movement of Fermi electrons. In Fig. 7, electrical conductivity calculated for $N = 5$, extended in y-direction where N is number of line defects. In this figure each point of graphs in Fig. 7 is the mean value of 50 calculation for random input variables. In diagram (7a) for 400meV incident electron energy, there is very little difference between the mean values of electrical conductivity in the random case, $\overline{\frac{G}{G_0}}$, and its counterpart in regular superlattice, $\frac{G}{G_0}$. In Fig. 7a at 180meV incident electron energy, for those values of d which is nearly less than 10\AA there is a large difference between the electrical conductivities in random and regular cases. After 10\AA , there is no difference between these two values, because of interference of different modes. In diagram (7b), in solid line curves where the strength of potential barriers are random, electrical conductivity has a large difference with its counterpart in regular case, plotted by dashes line curves. Electrical conductivity in averaged mode, at least in a wide range of U is larger than electrical conductivity in regular superlattice. This behavior is due to the constructive interference of modes, caused by random distance between barriers. There are well-defined peaks which decrease and increase with increasing the thickness of the central layer of the structure. This behavior is a result of resonant tunneling through structure and

quantum-well states formed in the central layer [29], [30], [31], [32].

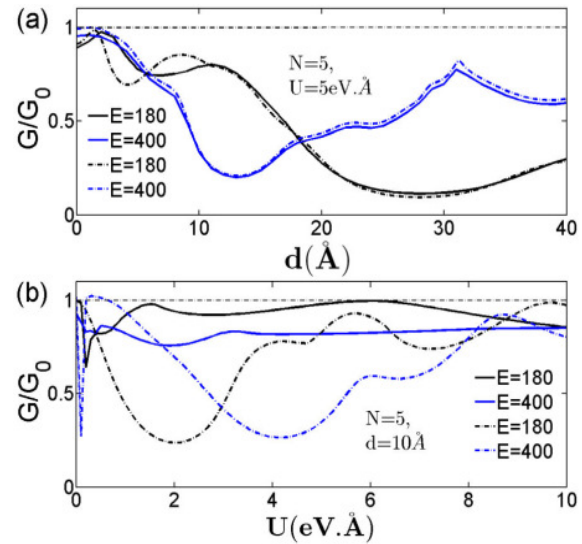


Figure 7. Diagram (a) is Electrical conductivity in terms of distance between barriers and diagram (b) is Electrical conductivity in terms of potential strength.

4 Conclusions

In summary, we compared transmission coefficients and electrical conductivities of two cases: random potential include potential strength and lattice constant, with regular superlattice. In both cases we used the Dirac delta-function form for potential barriers. By changing the structural parameters such as, potential heights, distance between barriers, energy of incident electrons, and direction of incident electrons significant differences are seen in the transmission coefficients and electrical conductivity for random and regular cases. Generally, randomness of potential and interfering between the transmitted and reflected electron waves are responsible for these behaviors. In electrical conductivity, there are more differences between the averaged values of random superlattice and fixed values of regular superlattice. In a situation where the lattice constant is random, the mean value of electrical conductivity is higher than its counterpart with fixed lattice constant. This suggests that random potentials can be closer to the real behavior of surface conduction in the Bi_2Te_3 topological insulator. Therefore, by creating random potential barriers, the electrical conductivity of incident electrons is

improved. Defect resonance modes have been reported by STM (scanning tunneling microscopy) for incident energies less than 200meV above the Dirac point surface [12], [33], [34]. This formalism can be generalized to the infinite random potential barrier on the surface of these insulators.

References

- [1] X. Qi, S. Zhang, "Topological Insulators and Superconductors." *Reviews of Modern Physics*, **83** (2011) 1057.
- [2] X. Qi, S. Zhang, "The Quantum Spin Hall Effect and Topological Insulators." *Physics Today*, **63** (2010) 33.
- [3] L. Fu, C.L. Kane, "Topological Insulators with Inversion Symmetry." *Physical Review B*, **76** (2007) 045302.
- [4] L. Fu, C. L. Kane, E. J. Mele, "Topological Insulators in Three Dimensions." *Physical Review Letters*, **98** (2007) 106803.
- [5] C. L. Kane, E. J. Mele, "Z₂ Topological Order and the Quantum Spin Hall Effect." *Physical Review Letters*, **95** (2005) 146802.
- [6] C. L. Kane, E.J. Mele, "Hall and Spin Hall Viscosity in 2D Topological Systems." *Physical Review Letters*, **95** (2005) 146801.
- [7] N. Nagaosa, "A New State of Quantum Matter." *Science*, **318** (2007) 758.
- [8] J.E. Moore, L. Balents, "Topological Invariants of TimeReversal-Invariant Band Structures." *Physical Review B*, **75** (2007) 121306(R).
- [9] J.E. Moore, "Topological insulators: The Next Generation." *Nature Physics*, **5** (2009) 375.
- [10] Q. Liu, C-X. Liu, C. Xu, X-L. Qi, S.C. Zhang, "Magnetic Impurities on the Surface of a Topological Insulator." *Physical Review Letters*, **102** (2009) 156603.
- [11] A.A. Zyuzin, D. Loss, "RKKY Interaction on Surfaces of Topological Insulators with Superconducting Proximity Effect." *Physical Review B*, **90** (2014) 125443.
- [12] Y. Xu, J. Chiu, L. Miao, H. He, Z. Alpichshev, A. Kapitulnik, R.R. Biswas, L.A. Wray, "Disorder Enabled Band Structure Engineering of a Topological Insulator Surface." *Nature Communications*, **8** (2017) 14081.
- [13] L. Miao et al, "Observation of a Topological Insulator Dirac Cone Reshaped by Non-Magnetic Impurity Resonance." *npj Quantum Materials*, **3** (2018) 29.
- [14] Y. K. Kato, R. C. Myers, A. C. Gossard, D. D. Awschalom, "Observation of the Spin Hall Effect in Semiconductors." *Science*, **306** (2004) 1910.
- [15] H. J. Zhang, C. X. Liu, X. L. Qi, X. Dai, Z. Fang, S. C. Zhang, "Topological Insulators in Bi₂Se₃, Bi₂Te₃ and Sb₂Te₃ with a Single Dirac Cone on the Surface." *Nature Physics*, **5** (2009) 438.
- [16] M. Z. Hassan, C. L. Kane, "Colloquium: Topological Insulators." *Reviews of Modern Physics*, **82** (2010) 3045.
- [17] Y. Xia et al., "Observation of a Large-Gap Topological-Insulator Class with a Single Dirac Cone on the Surface." *Nature Physics*, **5** (2009) 398.
- [18] Y. Okada, W. Zhou, D. Walkup, C. Dhital, S.D. Wilson, V. Madhavan, "Ripple-Modulated Electronic Structure of a 3D Topological Insulator." *Nature Communications*, **3** (2012) 1158.
- [19] H. Li, J. M. Shao, H. B. Zhang, D. X. Yao, G. W. Yang, "Resonant Tunneling in a Topological Insulator Superlattice." *Journal of Applied Physics*, **114** (2013) 093703.
- [20] J. An, C.S. Ting, "Surface States Scattering From a Step Defect in the Topological Insulator Bi₂Te₃." *Physical Review B*, **86** (2012) 165313.
- [21] D. Zhang, C. S. Ting, "Impact of Step Defects on Surface States of Topological Insulators." *Physical Review B*, **85** (2012) 115434.
- [22] T. Chiba, S. Takahashi, G.W. Bauer, "Magnetic-Proximity-Induced Magnetoresistance on

- Topological Insulators." *Physical Review B*, **95** (2017) 094428.
- [23] M. Arabikhah, A. Saffarzadeh, "Surface State Transport in Double-Gated and Magnetized Topological Insulators with Hexagonal Warping Effects." *Journal of Physics: Condensed Matter*, **31** (2019) 445001.
- [24] H. Dehnavi, A.A. Masoudi, M. Saadat, H. Ghadiri, A. Saffarzadeh, "Electron Scattering in a Superlattice of Line Defects on the Surface of Topological Insulators." *Journal of Physics: Condensed Matter*, **32** (2020) 415002.
- [25] Y. L. Chen et al., "Experimental Realization of a Three-Dimensional Topological Insulator, Bi_2Te_3 ." *Science*, **325** (2009) 178.
- [26] L. Fu, "Hexagonal Warping Effects in the Surface States of the Topological Insulator Bi_2Te_3 ." *Physical Review Letters*, **103** (2009) 266801.
- [27] K. Kuroda et al, "Hexagonally Deformed Fermi Surface of the 3D Topological Insulator Bi_2Te_3 ." *Physical Review Letters*, **105** (2010) 076802.
- [28] U. Fano, "Effects of Configuration Interaction on Intensities and Phase Shifts." *Physical Review*, **124** (1961) 1866.
- [29] A. Saffarzadeh, "Tunnel magnetoresistance in double spin filter junctions." *Journal of Physics: Condensed Matter*, **15** (2003) 3041.
- [30] M. Chshiev, D. Stoeffler, A. Vedyayev, K. Ounadjela, "Magnetic Diode Effect in Double Barrier Tunnel Junctions." *Europhys.letters*, **58** (2002) 257.
- [31] A. Kalitsov, A. Coho, N. Kioussis, A. Vedyayev, M. Chshiev, and A. Granovsky, "Impurity-induced tuning of quantum well states in spin-dependent resonant tunneling" *Physical Review Letters*, **93** (2004) 046603.
- [32] M. Wilczynski, J. Barnas, "Tunnel magnetoresistance in ferromagnetic double-barrier planar junctions: Coherent tunneling regime." *Journal of Magnetism and Magnetic Materials*, **221** (2000) 373.
- [33] M. L. Teague et al., "Observation of Fermi-Energy Dependent Unitary Impurity Resonances in a Strong Topological Insulator Bi_2Se_3 with Scanning Tunneling Spectroscopy." *Solid state commun*, **152** (2012) 747.
- [34] Z. Alpichshev et al, "STM Imaging of Impurity Resonances on Bi_2Te_3 ." *Physical Review Letters*, **108** (2012) 206402.